Ru2 and *Ru* encode mouse orthologs of the genes mutated in human Hermansky-Pudlak syndrome types 5 and 6

Qing Zhang[1*], Baohui Zhao[1*], Wei Li[1*], Naoki Oiso[2*], Edward K. Novak[1], Michael E. Rusiniak[1], Rashi Gautam[1], Sreenivasulu Chintala[1], Edward P. O'Brien[1], Yuke Zhang[1], Bruce A. Roe[3], Rosemary W. Elliott[1], Eva M. Eicher[4], Ping Liang[5], Christian Kratz[6], Eric Legius[7], Richard A. Spritz[2], T. Norene O'Sullivan[8], Neal G. Copeland[8], Nancy A. Jenkins[8] & Richard T. Swank[1]

*These authors contributed equally to this work.

Published online 27 January 2003; doi:10.1038/ng1087

Hermansky-Pudlak syndrome (HPS) is a genetically heterogeneous disease involving abnormalities of melanosomes, platelet dense granules and lysosomes. Here we have used positional candidate and transgenic rescue approaches to identify the genes mutated in ruby-eye 2 and ruby-eye mice (*ru2* and *ru*, respectively), two 'mimic' mouse models of HPS. We also show that these genes are orthologs of the genes mutated in individuals with HPS types 5 and 6, respectively, and that their protein products directly interact. Both genes are previously unknown and are found only in higher eukaryotes, and together represent a new class of genes that have evolved in higher organisms to govern the synthesis of highly specialized lysosome-related organelles.

Introduction

HPS is a genetically heterogeneous, recessively inherited disease that affects several organs. Persons with HPS present with oculocutaneous albinism, low visual acuity, prolonged bleeding that may require multiple platelet transfusions, and, in many cases, fatal lung disease in midlife[1,2]. HPS is often a debilitating disease and has no known cure. These clinical problems stem from abnormalities in vesicle trafficking to and among subcellular organelles that include melanosomes, platelet dense granules and lysosomes[2].

The identification of genes involved in HPS in humans and mice has demonstrated the molecular genetic bases of HPS. Four genetically distinct types of human HPS have been described. The human gene *HPS1* corresponds to mouse *Hps1* (also known as pale ear, *ep*)[3–5]; *AP3B1* (*HPS2*), to *Ap3b1* (*pe*, pearl)[6,7]; *HPS3*, to *Hps3* (*coa*, cocoa)[8,9]; and *HPS4*, to *Hps4* (*light ear*)[10]. But many individuals with HPS lack mutations in known HPS-related genes[2]. A successful strategy to identify genes involved in HPS in humans has been first to identify such genes in mice, in which high-resolution genetic maps generated by large-scale backcrosses simplify subsequent molecular approaches. In mice, there are at least 16 naturally occurring hypopigmentation models of HPS[11,12], and 9 of these have been characterized at the molecular level.

Two of these HPS-like mouse mutants, ruby-eye (*ru*; mouse chromosome 19) and ruby-eye 2 (*ru2*; mouse chromosome 7), have a variety of abnormalities of lysosome-related organelles. In both of these mutants, the coat and eyes are hypopigmented; indeed, ruby-eye and ruby-eye 2 mice are completely indistinguishable in appearance[13]. Melanosomes of the ruby-eye mouse, first described in a silver piebald stock of Danforth[14], are widely divergent in size and shape[13]. The mimic *ru2* mutation occurred in a substrain of C57Bl, and several additional alleles[15,16] appeared in various inbred mouse strains. Although lysosomal morphology is normal in ruby-eye and ruby-eye 2 mice, kidney proximal tubule cells secrete lysosomal enzymes into urine at greatly reduced rates in both[17]. Platelet dense granules are very deficient in critical components such as serotonin and adenine nucleotides in both, leading to functionally abnormal platelets and prolonged bleeding times[18]. Another subcellular organelle, the mast cell granule, undergoes unregulated 'kiss-and-run' fusion at the plasma membrane of mast cells of ruby-eye mice[19]. Here we describe the identification of mouse *ru2* and *ru*, identify mutations in both of these genes in human patients with previously unclassified forms of HPS, and demonstrate that the ru and ru2 proteins directly interact in a previously unknown complex we have called biogenesis of lysosome-related organelles complex 2 (BLOC-2).

[1]*Department of Molecular and Cellular Biology, Roswell Park Cancer Institute, Buffalo, New York 14263, USA.* [2]*Human Medical Genetics Program, University of Colorado Health Sciences Center, Denver, Colorado 80262, USA.* [3]*Department of Chemistry and Biochemistry, University of Oklahoma, Norman, Oklahoma, USA.* [4]*The Jackson Laboratory, Bar Harbor, Maine, USA.* [5]*Department of Cancer Genetics, Roswell Park Cancer Institute, Buffalo, New York, USA.* [6]*Klinik für Pädiatrische Hämatologie und Onkologie, Heinrich-Heine-Universität, Düsseldorf, Germany.* [7]*Center for Human Genetics, Universitaire Ziekenhuizen Leuven, Leuven, Belgium.* [8]*Mouse Cancer Genetics Program, National Cancer Institute, Frederick, Maryland, USA. Correspondence should be addressed to R.T.S (e-mail: richard.swank@roswellpark.org).*

Results

Positional cloning of *ru2*

The gene *ru2* was previously mapped at low resolution near the 25 cM region of mouse chromosome 7 (refs. 15,20). To construct a high-resolution genetic map of the *ru2* gene region, we generated 1,568 [C57Bl/6J $ru2^J/ru2^J$ × *Mus musculus musculus* (PWK)] F1 × C57Bl/6J $ru2^J/ru2^J$ progeny and assigned scores to these mice for coat color and for a series of molecular markers that mapped near *ru2* (Fig. 1*a*). We constructed a physical map of the *ru2* interval from a contig of 16 overlapping BACs (Fig. 1*b*) and fully sequenced three BACs (116A10, 28A7 and 323L3) spanning this interval. We identified several known genes, including those encoding the serum amyloid A family, the downstream general transcription factor IIH polypeptide 1 and genes of the lactate dehydrogenase family, within these sequences by searching genomic human and mouse databases, establishing that this region is orthologous to human chromosome 11p13–15.

RT-PCR analysis of transcripts of one candidate gene, expressed sequence tag (EST) BF784343, showed obvious abnormalities of the $ru2^J$ allele in cDNA from kidney, spleen and brain (data not shown). Furthermore, we identified deleterious mutations in three *ru2* alleles by DNA sequencing (Table 1).

Positional cloning of *ru*

Previous low-resolution mapping[21] and an expanded analysis[3] of the *ru* region of mouse chromosome 19 used an interspecific backcross between the B6C3Fe- *bm ep ru/bm ep ru* laboratory stock and inbred strain PWK. We enhanced the genetic resolution of the map considerably (Fig. 1*c*) by including progeny from an intercross between strains JE/Le *a/a f/f je/+ ru/ru* and inbred strain CAST/Ei, yielding 2,221 total meioses, and mapped 46 microsatellite markers, known genes and other molecular markers in the two crosses (Fig. 1*c*). The closest (0.2 cM) proximal flanking marker recombinant with *ru* was the SP6 end of BAC 169B11. The closest (0.05 cM) non-recombinant distal flanking marker was the T7 end (*T500*) of PAC 500M11. Within a contig of seven BACs and two PACs, three BACs (169B11, 360P10 and 293M19) formed a minimum tiling path spanning the 0.25-cM (450-kb) critical *ru* interval (Fig. 1*d*).

We completely sequenced BAC 293M19 and identified four genes using database searches (Fig. 1*d*). The human homologs of these genes mapped to chromosome segment 10q24.32, the orthologous region for *ru*. Further analysis of this region using the Celera Gene Discovery system showed an unusual potential candidate gene whose entire open reading frame was encoded by a single exon.

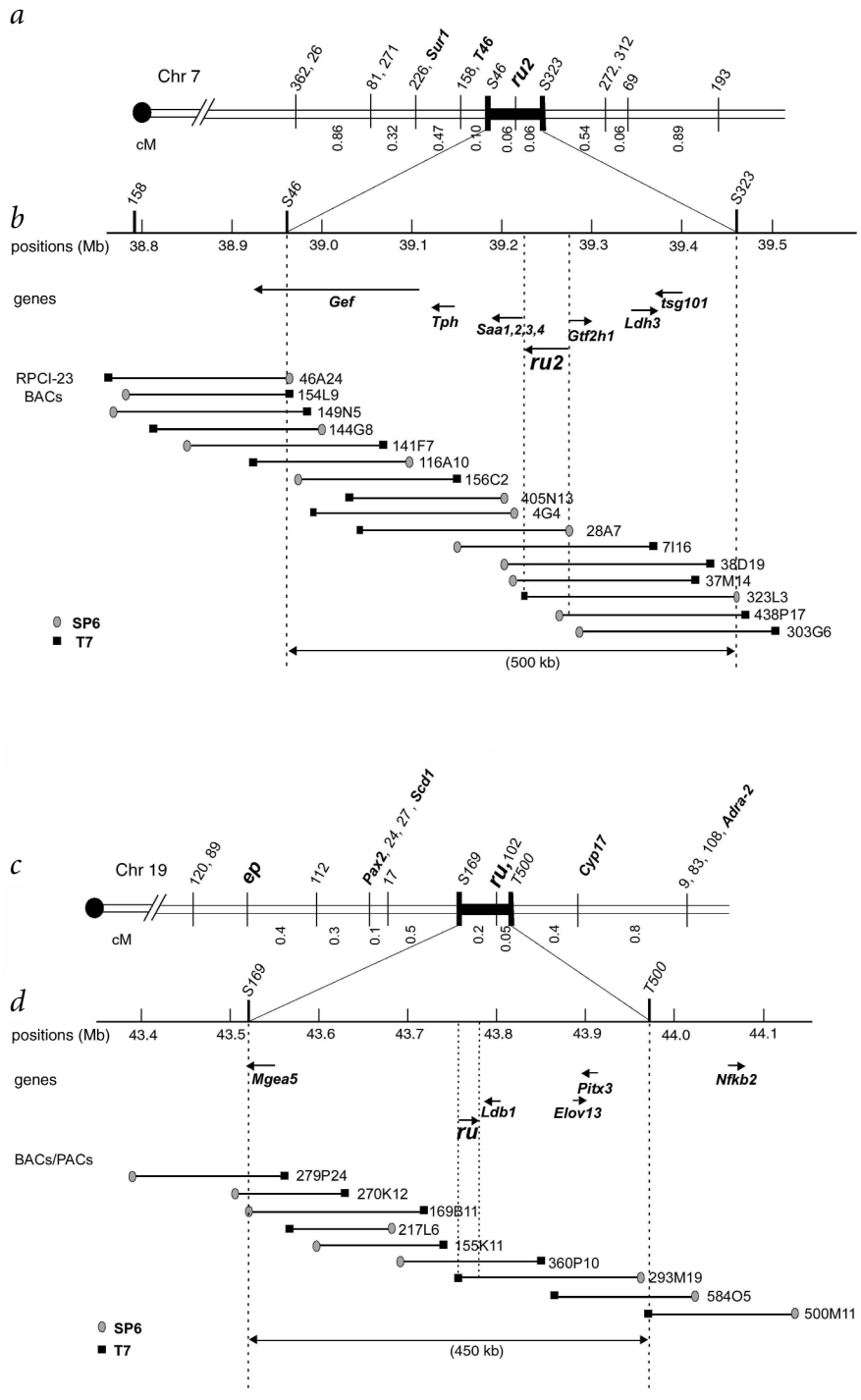

Fig. 1 High-resolution genetic (***a,c***) and physical (***b,d***) maps of the *ru2* and *ru* regions of mouse chromosomes 7 and 19. Genetic distances (*a*,*c*) between adjacent markers are given in map units (cM); centromeres (circles) are at left. Bolded molecular markers are expressed genes; numbered molecular markers are MIT microsatellites and single-nucleotide polymorphisms generated from BAC ends. Known genes and direction of transcription (arrows) are indicated in *b* and *d*. In *c*, *ep* indicates the pale ear (*Hps1*) gene on chromosome 19. Physical maps (*b*,*d*) span the *ru2* (500 kb) and *ru* (450 kb) critical genetic intervals (vertical dotted lines); gene positions are indicated in megabases (Mb). Mapped ends of BACs and PACs (*b*,*d*) are designated as T (T7) or S (SP6). All *ru2* BACs (B) are from the RPCI-23 BAC library. The *ru* BACs 217L6, 155K11, 360P10, 169B11 and 279P24 are from the Research Genetics CITB mouse BAC DNA Library. PACs 500 M11 and 584O5 are from the RPCI-21 library.

Table 1 • Deleterious mutations in mouse *ru2* and *ru* allelic mutants and in humans with HPS5 and HPS6

	Mutation	Mutation type
Mouse *ru2*^{J}	G757delGinsTT	frameshift
Mouse *ru2*^{hz}	E900insCCGG	frameshift
Mouse *ru2*	K867insTTTTTTTT……TTGAAACTGCCGCATCAAG (1-kb H2A histone)	insertion
Human *HPS5*	L675delAGTT	frameshift, homozygous
Mouse *ru*	H187-C188-P189del	in-frame deletion
Mouse *ru*^{3J}	W579X(1736G>A)	nonsense
Mouse *ru*^{4J}	G64delCCTGCCGCTG……TTCGTGCCGTG (66 nt)	in-frame deletion
Mouse *ru*^{6J}	M108insTGTGGGAAGCCGCCC……ACGCGTCAAATAACAGGGATG (~5.3 kb IAP element)	insertion
Human *HPS6*	C571delTCTG	frameshift, homozygous

The mutation in the *ru2*^{J} allele leads to a predicted loss of 311 amino acids at the C terminus. The *ru2*^{hz} allele mutation leads to a predicted loss of 118 C-terminal amino acids. The *ru2* allele contains a 1.0-kb insertion of the H2A histone sequence immediately preceding codon 868 of exon 18, with an eight-nucleotide duplication (underlined) 3′ to the insertion. The *ru* mutation results in loss of histidine, cysteine and proline at positions 187–189. The nonsense mutation in the *ru*^{3J} allele is expected to produce a truncation of 227 C-terminal amino acids. An in-frame deletion (confirmed by genomic PCR, not shown) of 66 nucleotides (nucleotides 192–257) of *ru*^{4J} predicts a loss of amino acids 65–86. An IAP of ~5.3 kb is inserted in the sense orientation at nucleotide position 324 of the *ru*^{6J} allele with a six-nucleotide insertion site duplication (underlined). The IAP insertion causes loss of expression of the normal kidney *ru*^{6J} transcript and expression of a larger (8.5-kb) transcript in brain (Fig. 3).

We initially obtained evidence for the relevance of this gene to *ru* by PCR amplification of genomic DNA. Qualitative or quantitative abnormalities (data not shown) were evident for several *ru* alleles, including an apparent partial deletion in *ru*^{4J} and an undetectable PCR product for *ru*^{6J}. We confirmed that this was *ru* by identifying deleterious mutations in all four *ru* alleles by direct sequencing of genomic DNA (Table 1).

Transgene rescue

Functional tests of candidate genes, especially those using whole animals, provide strong confirmatory evidence of their identities and *in vivo* functions. Injection of the *ru2* BAC 323L3 into homozygous *ru2*^{J} blastocysts produced 13 mice that were ru2 in coat color and 2 mice that were wild type in coat color (Fig. 2). Similarly, injection of the *ru* BAC 293M19 into homozygous *ru* blastocysts produced mice that were wild type as well as mutant in coat color (Fig. 2). These results show that BACs 323L3 and 293M19 contain *ru2* and *ru*, respectively. When combined with the mutation data described above, our results indicate that we have identified the correct genes and that both genes are essential for normal melanosome biogenesis and trafficking *in vivo*.

Expression of *ru2* and *ru*

All tissues examined expressed the wild-type 4.8-kb *ru2* mRNA (see Web Fig. A online), which was consistent with the presence of lysosomes in all tissues. There was less expression in skeletal muscle and spleen. We found no differences between the northern blot patterns of tissues of *ru2*^{J}/*ru2*^{J} mice (which have a frameshift mutation (Table 1) in *ru2*) and those of normal mice (data not shown), indicating that this mutant mRNA is not subject to 'nonsense-mediated' decay. Using 5′ rapid amplification of cDNA ends (RACE), we found additional *ru2* transcripts arising from alternative splicing in normal mouse kidney. These included a transcript (AF534398) predicted to encode a 961-amino-acid in-frame ru2-related protein truncated by 165 amino acids at its N terminus and another transcript (AF534399) encoding an in-frame ru2-related protein of 526 amino acids truncated by 600 amino acids at its C terminus. In human placenta, two additional transcripts (AF534400 and AF534402), arising from alternative splicing, probably encode a slightly smaller in-frame protein that contains 114 fewer amino acids at the N terminus because of the use of an alternative translation start site. Whether all the several proteins potentially encoded by the various mouse and human alternative transcripts are actually expressed is not known.

The 2.6-kb *ru* mRNA was also expressed (see Web Fig. A online) in all tissues tested; again, levels were reduced in skeletal muscle. Northern blot analysis (Fig. 3) demonstrated an aberrant (8.5-kb) *ru* mRNA in the brains of mice carrying the *ru*^{6J} allele, consistent with the insertion of an intracisternal A particle (IAP) element (Table 1). Furthermore, the IAP insertion had a profound effect in the kidney, in which there was only a very low level of high-molecular-weight *ru* transcript in homozygous *ru*^{6J} mice.

Properties of the *ru2* and *ru* gene products

Mouse *ru2* is relatively large (42,656-base-pair (bp) genomic and 4,610-bp cDNA with an open reading frame of 3,381 bp), consisting of 23 exons ranging in size from 66 bp (exon 4) to 985 bp (exon 23). The organization of the corresponding human gene is identical, with 23 exons and 22 introns.

Fig. 2 Transgenic 'rescue' of *ru2* and *ru*. Fertilized eggs homozygous with respect to *ru2*^{J} or *ru* were injected by transgenic techniques with BAC 323L3 or BAC 293M19, respectively. The litters shown here include one rescued black pup (*) plus ruby-eye 2 or ruby-eye littermates who did not receive the transgene. We molecularly verified the presence of the appropriate injected BAC in each rescued black pup.

The encoded mouse ru2 protein (Fig. 4*a*) contains 1,126 amino acids (126.3 kDa); the corresponding human protein contains 1,129 amino acids (127.4 kDa). Mouse ru2 is 81% identical to the orthologous human sequence. We found low identity (26%) between 111 amino acids at the N termini of the mouse and *Drosophila melanogaster* (AAF54263) proteins. Likewise, we found low identity (26%) between 403 amino acids at the N termini of the mouse protein and a worm (*Caenorhabditis elegans*) protein (T26318). The worm protein is unusual in that it contains a large (516-amino-acid) extension at the N terminus, which is not found in the mammalian proteins. Finally, we found 49% identity between mouse ru2 and a fugu fish (*Takifugu rubripes*) protein (BK000665).

Mouse *ru* and its human homolog are unusual in that they contain a relatively large open reading frame (2,418 bp), together with small amounts of 5′ (93-bp) and 3′ (110-bp) untranslated sequences, all within a single exon. We identified EST sequences representing partial coding sequences of orthologous *ru* genes from other vertebrate species, including rat, cow, chicken and fish. Mouse (AF536239) and human (AF536238) *ru* cDNA sequences are 78% identical within the open reading frames.

Mouse *ru* encodes an 88.8-kDa protein of 805 amino acids (Fig. 4*b*). The translated protein products of mouse *ru* and its human homolog are 80% identical, and those of mouse and rat *ru* are 92% identical. We detected a more distantly related (31% identical) homolog (BK000659) in the fugu fish (*Takifugu rubripes*). The mouse and rat (BK000658) proteins (805 residues) are somewhat larger than the corresponding human protein (775 residues). The main difference between the rodent and human species occurs at the C terminus, where the rodent proteins have an extension of 31 residues.

Proteins homologous to either ru2 or ru are not apparent in lower eukaryotes such as yeast. Database analyses indicate that both ru2 and ru are previously unknown, with no common domains, signal sequences or transmembrane domains, with the exception (at low statistical likelihood) of two WD40 domains at amino acids 65–105 and 113–153 of ru2.

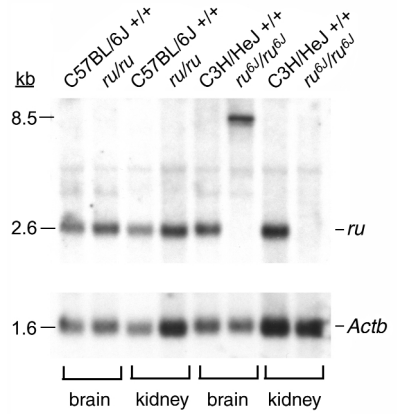

Fig. 3 Transcripts of the ru^{6J} allele are abnormally expressed in kidney and brain. We probed northern blots of kidney and brain RNA from *ru/ru* and ru^{6J}/ru^{6J} mice, and mice of their respective control inbred strains C57Bl/6J and C3H/HeJ, with *ru* (top) or β-actin (bottom) probes. +/+ indicates $ru^{+/+}$ (wild type). Left margin, molecular size indicators.

a

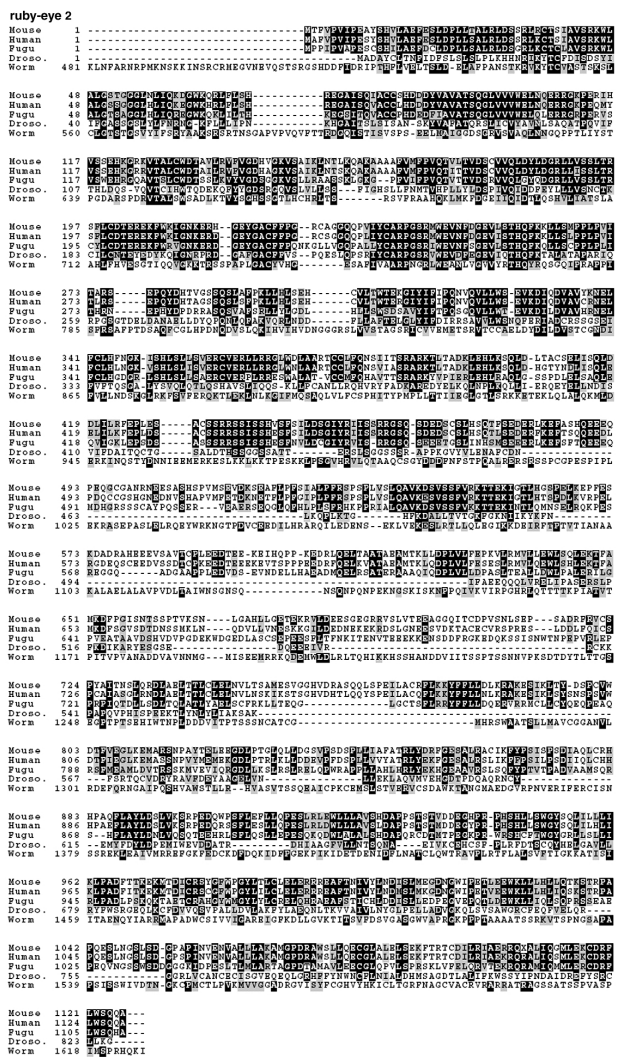

b

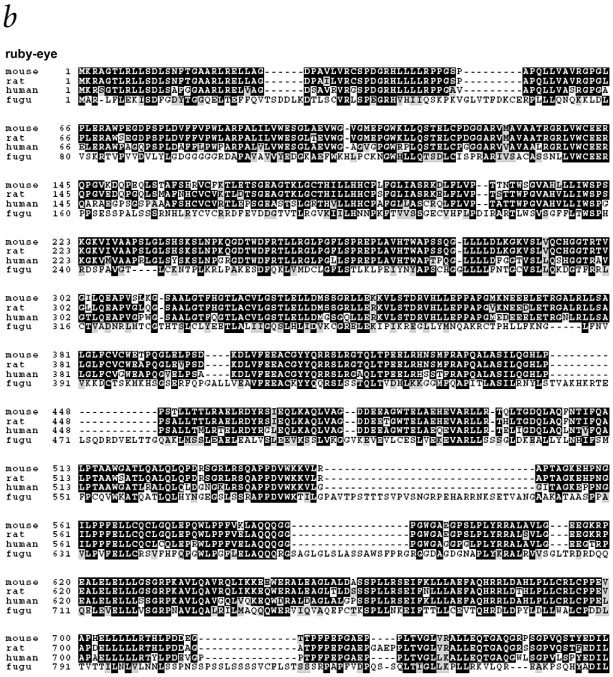

Fig. 4 Alignment of mouse ru2 (***a***) and ru (***b***) sequences with orthologous sequences from other species. Dark-shaded residues are identical; light-shaded residues are similar; unshaded residues differ. Droso., *Drosophila melanogaster*. Left margins, amino-acid positions.

Mutations in *ru2* and *ru* homologs in humans

Most Puerto Ricans with HPS have mutations in *HPS1* (ref. 5) or *HPS3* (ref. 9). However, among non-Puerto Ricans with HPS, about half have mutations in *HPS1*, and about one-sixth in *HPS4* (ref. 10), whereas about one-third do not have detectable mutations in the genes previously known to be involved in HPS. We screened for mutations of the human *ru2* and *ru* homologs in 20 such non-Puerto Ricans with HPS, and found pathologic mutations of these genes in one individual each, establishing the human *ru2* and *ru* homologs as *HPS5* and *HPS6*, respectively.

The individual with HPS type 5 (HPS5) was a 3-year-old Turkish boy with clinically mild oculocutaneous albinism and easy bruising. His platelet count was moderately reduced, at 102,000/mm^3, and his bleeding time was moderately prolonged, at 7 minutes 20 seconds. Platelet function tests showed reduced aggregation in response to ADP and reduced ATP secretion in response to collagen. The individual's parents were first cousins, and he had a brother who was unaffected. Single-strand conformation polymorphism (SSCP)–heteroduplex[22] and DNA sequence analyses identified a homozygous four-base-pair deletion (of AGTT) at codons L675–V676 (TTAGTT→TT) of the human gene orthologous to *ru2*, resulting in a frameshift with truncation of the nonsense polypeptide at codon 682, causing loss of 40% of ru2 at the C terminus.

The individual with HPS6 was a 39-year-old Belgian woman with oculocutaneous albinism and frequent prolonged nosebleeds, as well as prolonged bleeding after dental extractions and surgery. She had no pulmonary or gastrointestinal symptoms. Her platelet count was normal, and her bleeding time was moderately prolonged, at 6 minutes 30 seconds. Platelet function tests showed reduced secretion in response to ATP. Electron microscopy of her platelets showed only very rare dense granules. Her parents had no known consanguinity, but both were from the same small region of east Flanders (Belgium); a brother was similarly affected. SSCP-heteroduplex[22] and DNA sequence analyses identified a homozygous four-base-pair deletion (of TCTG) in codons C571–L572 (TGTCTG→TG) of *ru*, resulting in a frameshift with truncation of the nonsense polypeptide at codon 610, causing loss of 30% of ru at the C terminus.

Melanosomal abnormalities in *ru2* and *ru* mice

Because individuals with HPS and ruby-eye 2 and ruby-eye mice have hypopigmentation, we did electron microscopic analyses of melanosomes of the retinal pigment epithelium (RPE) and choroid of the eye. The *ru2* mutation causes notable quantitative and qualitative abnormalities of the melanosomes of the RPE and choroid (Fig. 5). The RPE of mutants contains greatly reduced numbers of melanosomes. The remaining RPE melanosomes are often morphologically bizarre, containing multilamellar or granular inclusions, whereas others have rough edges. Choroidal melanosomes of mutants are often misshapen and less dense than normal. A distinctive feature (Fig. 5) not found in the melanosomes of other pigment mutants[3,8,10,23] is a tendency for choroidal melanosomes to be clumped within multimelanosomal bodies.

Abnormalities of the RPE and choroid of ruby-eye mice seemed essentially identical to those of ruby-eye 2 mice. Quantitative and qualitative abnormalities of melanosomes of both tissues were apparent. Melanosomes in each tissue were greatly reduced in number, especially in the RPE. Remaining mutant RPE melanosomes were often disorganized. In the choroid, melanosomes often had ragged outlines rather than the smooth exterior membranes found in normal cells. A most salient feature was the clumping of ruby-eye choroidal melanosomes, like those of the ruby-eye 2 choroid, within large multimelanosomal bodies.

Interaction of ru2 and ru

The fact that the ru2 and ru mutants have mimic gene mutations[13] indicates that the proteins encoded by these genes might interact in the same pathway or even in the same protein complex. A combination of co-immunoprecipitation and yeast two-hybrid approaches (Figs. 6 and 7) confirmed that the proteins indeed interact.

We co-transfected COS-7 cells with epitope-tagged cDNA constructs of *ru2* and *ru* (Fig. 6), or with one of these constructs paired with cDNA constructs of the genes *pe* (*Ap3b1*) or *STAT3*, as negatively interacting controls. Western blot analyses of transfected cells (inputs) showed substantial expression of the Flag (Fig. 6*a*) and Myc (Fig. 6*b*) constructs of all cDNAs and the expected proteins

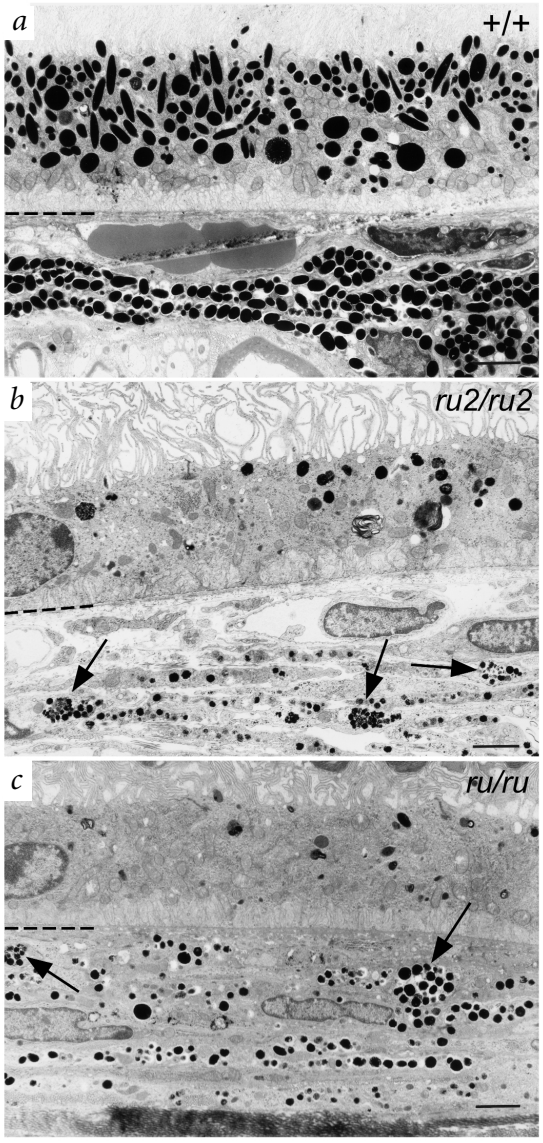

Fig. 5 Melanosomes of the retinal pigment epithelium (RPE) and choroid (CH) are quantitatively and qualitatively abnormal in eyes of ruby-eye 2 and ruby-eye mutants. Samples are from normal C57Bl/6J (***a***), ruby-eye 2 (***b***) and ruby-eye (***c***) mice. Arrows indicate large clumps of melanosomes within a single membrane-limited body in the ruby-eye 2 and ruby-eye choroids. Scale bars, 2 μm. The interface between the RPE (above) and CH regions (below) is indicated by the hyphenated partial line at the left.

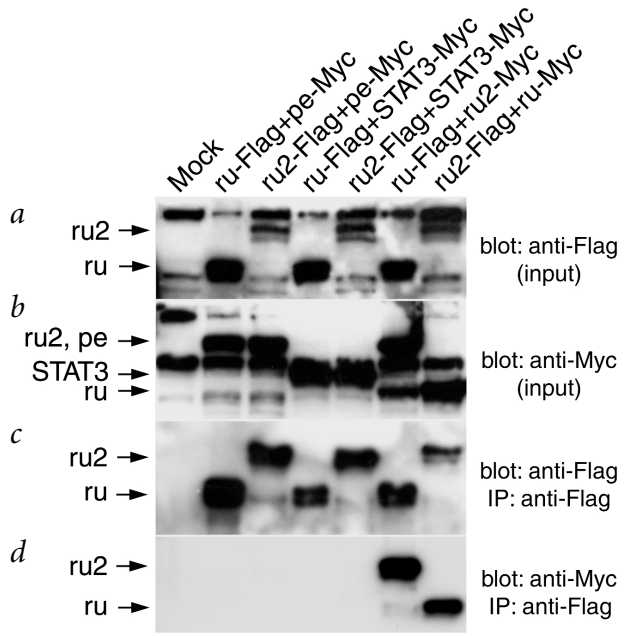

Fig. 6 The ru2 and ru proteins are components of a complex. We co-transfected COS-7 cells with epitope-tagged constructs expressing the indicated proteins and analyzed them by western blot 48 h after transfection. We immunoprecipitated proteins in *c* and *d* with Flag M2 antibody–conjugated agarose. ***a***, Flag in total lysates (10% of the total lysate) detected by polyclonal antibody against Flag. ***b***, Myc in total lysates (10% of the total lysate) detected by polyclonal antibody against Myc. ***c***, Immunoprecipitated Flag protein (75% of lysate) detected by polyclonal antibody against Flag. ***d***, Specific interaction between ru2 and ru (75% of lysate) detected by antibody against Myc. Left, mobility positions of ru, ru2, pe and STAT3.

within the Flag immunoprecipitates (Fig. 6*c*). Western blot analyses of Flag precipitates analyzed with the Myc antibody showed co-immunoprecipitation of ru2 and ru (Fig. 6*d*). A considerable percentage of the ru2-Myc and ru-Myc proteins were co-immunoprecipitated by antibodies against the ru-Flag and ru2-Flag proteins, respectively. In contrast, there was no visible co-precipitation of either the pe-Myc or the STAT3-Myc proteins by antibodies against either the ru-Flag or the ru2-Flag proteins.

Yeast two-hybrid analyses (Fig. 7) showed that ru2 and ru interact directly in this system whether their cDNAs are inserted in the binding or activation domains. There was no direct interaction between another protein involved in HPS (Hps3) and either ru2 or ru.

Discussion

The identification of genes involved in HPS in humans and mice is enhancing knowledge of the molecular genetic bases of this disease. Altogether, 11 mouse and 6 human genes involved in HPS have been identified at the molecular level. A useful generality is that the HPS genes fall into two classes. The first class includes five genes, *Ap3d*, *Ap3b1*, *Rabggta*, *Rab27a* and *Vps33a*, encoding proteins known to regulate vesicle trafficking: respectively, the δ (mocha)[24] and β-3A (pearl)[6] subunits of the AP-3 adaptor complex[25], the α subunit of the Rab geranylgeranyl transferase enzyme (gunmetal)[26], ashen[27–31], and buff[32], the *Vps33a* subunit of the class C complex. The second class consists of seven newly identified genes: *HPS1* (*ep*)[3–5], pallid (*pa*)[33], muted (*mu*)[23], *HPS3* (*coa*, cocoa)[8,9], *HPS4* (light ear)[10] and now *HPS5* (ruby-eye 2) and *HPS6* (ruby-eye). Proteins of the second class are of interest because they are previously unknown, they are found only in higher eukaryotes, and the mechanisms by which they regulate vesicle trafficking are largely unknown. The existence of this class indicates that a new group of genes has evolved to regulate the synthesis and function of lysosomes and of highly specialized eukaryotic organelles such as melanosomes and platelet dense granules.

Although ru and ru2 are newly identified, the nature of the mutation in the *ru* allele indicates that the region of ru that includes amino acids 187–189 (His-Cys-Pro) is functionally important. The nine-base-pair deletion in the *ru* allele is minimal and in-frame, is in a conserved region of the protein (Fig. 4*b*) and does not alter mRNA levels (see Web Fig. A online). As in other mouse HPS mutants, expression of *ru2* and *ru* mRNA is ubiquitous, consistent with the fact that HPS is a multi-organ disease and that lysosomes are present in all tissues. Clearly, the transgene rescues and the morphological abnormalities of eye melanosomes documented here indicate that both genes have considerable influence on the biogenesis and trafficking of this organelle. Both *ru2*/*ru2* and *ru*/*ru* mice have identical clumping of melanosomes within a single body in choroidal tissue, a phenomenon not found in other mouse HPS mutants[3,8,10,23,24]. The fact that the mimicry of *ru2* and *ru* extends to such fine details of melanosome malformation indicates that these two genes affect the same or closely related vesicle trafficking pathway(s), consistent with the mimic nature of these mutations with regard to coat color, platelet dense granules and lysosome secretion. The HPS phenotype is relatively mild in both ruby-eye 2 and ruby-eye mice[17], and in the individuals with HPS5 and HPS6 described here. These facts are also consistent with the likelihood that the two genes affect similar biosynthetic and trafficking pathways in both species.

The co-immunoprecipitation and yeast two-hybrid analyses indicate that ru2 and ru interact directly in a protein complex. Whereas the detailed mechanisms by which proteins involved in HPS regulate the synthesis of lysosome-related organelles remain unknown in most cases, a developing theme is that they act in concert with other HPS-related proteins in protein complexes. The Ap3b1 and Ap3d proteins are components of the well-studied AP-3 adaptor complex[25]. Other newly identified and less well-studied proteins involved in HPS contribute to other protein complexes. For example, the muted and pallidin proteins are included in the BLOC-1 complex[34,35]. We accordingly propose that the Hps5-Hps6 (ru2-ru) complex be called BLOC-2. Genetic and subcellular fractionation evidence, combined with indications of secondary interaction, indicate complex formation between the Hps1 and Hps4 proteins[10,36,37]. Additional studies are required to determine if any proteins involved in HPS are shared among the three complexes.

Yeast two-hybrid approaches[38] indicate that a human protein orthologous to mouse ru2 binds to the conserved region of the cytoplasmic domain of the α3A integrin subunit. However, we have been unable to replicate this result using the Clontech Matchmaker 3 yeast two-hybrid system.

The identification of *ru2* and *ru* should eventually lead to an understanding of the mechanisms by which these two genes regulate the synthesis of lysosome-related organelles. Molecular studies of their interaction with the dilute suppressor gene (*dsu*), which suppresses the hypopigmentation of the choroid of the eyes of ruby-eye 2 and ruby-eye mice[39], are now possible. Likewise, the identification of *ru* should elucidate the mechanism(s) by which it regulates fusion of mast cell granules with the mast cell plasma membrane at the mast cell exocytotic fusion pore[19]. The availability of the *HPS5* and *HPS6* sequences substantially increases the probability of identifying responsible gene mutations in known but presently undiagnosed individuals and in those newly diagnosed with HPS. They also will be useful in future gene therapy experiments and in showing the unique molecular processes affecting vesicle trafficking to and among lysosome-related organelles.

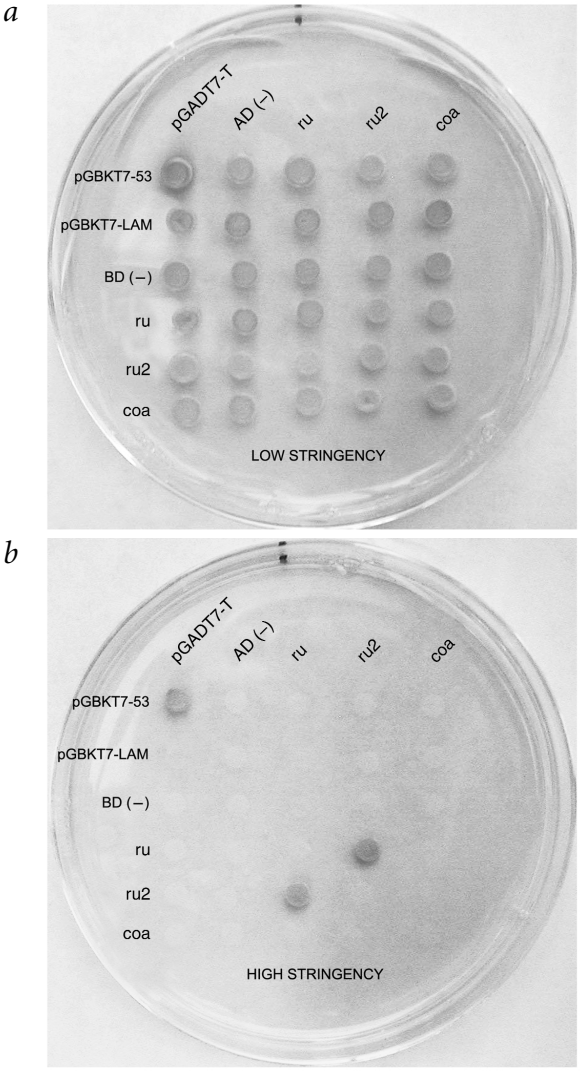

Fig. 7 The ru2 and ru proteins directly interact. We transformed yeast strain AH109 with constructs expressing the indicated proteins fused to binding domains (left) or activation domains (top). We spotted co-transformants on plates containing low-stringency (***a***) or high-stringency (***b***) medium and assessed interaction of proteins by growth and blue color on high-stringency plates. Co-transformants pGBKT7-53 and pGADT7-T are a positive control for interacting proteins; pGBKT7-LAM and pGADT7-T are a negative control.

Methods

Mice, genetic crosses and genomic DNA. We obtained ruby-eye 2 ($ru2^J/ru2^J$), ruby-eye (ru/ru and ru^{6J}/ru^{6J}) and control C57Bl/6J mice from The Jackson Laboratory and subsequently bred them in the animal facilities of Roswell Park Cancer Institute. All procedures (mouse protocol 125M) were reviewed and approved by the Roswell Park Institutional Animal Care and Use Committee, and adhered to the principles of the National Institutes of Health Guide for the Care and Use of Laboratory Animals.

We phenotyped progeny from a backcross between $ru2^J/ru2^J$ homozygous mice and inbred PWK wild-type mice by coat color, and genotyped them with microsatellite markers obtained from Research Genetics. We obtained a high-resolution genetic map of the region surrounding *ru* on mouse chromosome 19 by combining two crosses. The first was a backcross of 1,197 progeny[3,21] produced by first crossing the *M. musculus musculus* inbred strain PWK and an inbred laboratory stock homozygous with respect to *ep* (*HPS1*) and *ru*, and then backcrossing resulting heterozygous offspring to the B6C3Fe stock, which is homozygous with respect to *ep* and *ru*. The second cross was an intercross of 524 progeny between heterozygous F1 progeny of the JE/Le *ru/ru* inbred laboratory strain and the inbred *Mus musculus castaneus* strain CAST/Ei. We obtained genomic DNA samples from *ru2/ru2* (control strain, C57Bl/6J), $ru2^{hz}/ru2^{hz}$ (control strain, C57Bl/6J), *ru/ru* (control strain, C57Bl/6J), ru^{3J}/ru^{3J} (control strain, C57Bl/6J), ru^{4J}/ru^{4J} (control strain, SSL/Le), and ru^{6J}/ru^{6J} MICE (control strain, C3H/HeJ) from The Jackson Laboratory.

Genetic and physical maps. We generated genetic and BAC-based physical maps of the *ru2* critical region as described before[3,6,21]. We screened the RPCI-23 BAC library (Roswell Park Cancer Institute) with microsatellite markers and BAC end probes derived from the *ru2* critical genetic region. We subjected positive BACs to restriction enzyme digestion (*Not*I) and pulsed-field gel electrophoresis to determine insert size, and determined overlap among BACs by 0.8% agarose gel electrophoresis after digestion with *Eco*RI. We used PCR primer pairs designed from the BAC end sequences to construct a BAC contig of the *ru2* critical region. We isolated BACs within the *ru* critical region by screening the pBeloBAC11 CITB library from Research Genetics. We isolated PACs from the RPCI-21 library. We genotyped microsatellites for polymorphisms by PCR protocols, and a few other markers by Southern blot analysis of DNA from informative mouse samples containing crossovers in the *ru2* or *ru* critical genetic regions.

Sequencing and analyses of BACs and PACs. We sequenced BAC and PAC ends with SP6 and T7 promoter primers in the Roswell Park Cancer Institute Biopolymer Facility as described before[40]. We completely sequenced three BACs from the *ru2* critical genetic region (rp116A10, rp28A7 and rp323L3) and one BAC from the *ru* critical genetic region (BAC 293M19) at the University of Oklahoma Genome Center by standard optimized BAC shotgun sequencing methods[41,42] and assigned them GenBank accession numbers AC090652, AC090122, AC090123 and AC108484, respectively. We annotated BAC sequences by subjecting the working-draft sequences to BLAST searches after masking repetitive sequences. We used the entire sequence of BAC 293M19 to search the GenBank and Celera databases. We analyzed protein sequences and domain structures using the Network Protein Sequence Analysis server, the UK HGMP Resource Centre and SMART servers.

Sequencing of *ru* genomic DNA. We amplified the different *ru* alleles from genomic DNA and did control PCR amplifications of the mouse HPS-related gene muted (*mu*)[23] on the same genomic DNA. Primer sequences are available on request. The large size of the *ru* gene necessitated use of the Advantage 2 PCR Kit (Clontech Laboratories) for amplification. We sequenced products on an ABI Prism 377 DNA Sequencer as described before[39].

Cloning of mouse *ru* and the human homolog. We identified 64 mouse ESTs and 17 known genes by searching databases against the sequences of BACs 116A10, 28A7 and 323L3. We designed primers derived from the sequences of known ESTs and genes to screen for mutations among all three *ru2* alleles (primer sequences available on request). These amplifications identified a band shift within the *ru2* mutant, making this EST a candidate for *ru2*. We obtained the full-length EST sequence by sequencing the IMAGE clone 4238164. We used 5′ RACE of mouse kidney poly(A)$^+$ mRNA to extend the 5′ end of the EST (SMART RACE cDNA Amplification kit, Clontech) with two gene-specific primers (sequences available on request). We identified the 3′ end of mouse *ru2* by EST alignment and Celera database searching.

A BLAST query identified the BAC NT009307 as containing homologous human sequences. We designed primers (sequences available on request) from EST KIAA1017 to amplify the 5′ cDNA ends of human placental cDNA derived from poly(A)$^+$ mRNA (Clontech). We determined the genomic sequence of mouse *ru2* by alignment of the cDNA sequence with the sequence of BAC rp23-323L3 and the corresponding sequence from the Celera database. We determined the genomic sequence of the human *ru2* homolog by alignment of the cDNA sequence with the corresponding Celera database sequence.

Mutation analyses. We amplified the 23 coding exons of mouse or human *ru2* from genomic DNA of $ru2^J/ru2^J$, $ru2^{hz}/ru2^{hz}$ and *ru2/ru2* mice and the appropriate control strain C57Bl/6J, or individuals with HPS and controls, by PCR using primers derived from adjacent noncoding and intervening sequences. PCR products showing aberrant patterns were re-amplified and sequenced directly. We subjected PCR products from

humans to simultaneous SSCP-heteroduplex screening[22]. We amplified and then sequenced the single-exon *ru* gene from genomic DNA of the various *ru* alleles using long-range PCR protocols.

Expression analysis. We prepared total RNA and reverse transcribed it as described before[23]. For northern blot analysis of *ru2* transcripts, we used ^{32}P-radiolabeled probes generated by RT-PCR amplification of mouse or human RNA (primer sequences available on request). For northern blot analysis of *ru* transcripts, we generated a transcript-specific 524-bp *ru* probe by RT-PCR amplification of total RNA from C57Bl/6J brain (primer sequences available on request). We used ExpressHyb Hybridization Solution (Clontech) according to manufacturer's instructions. The mouse multiple-tissue northern blot was purchased from Clontech.

Electron microscopy. We did electron microscopy as described before[23]. We fixed, dehydrated and embedded eye tissue samples in Spurr resin, cut the samples into sections 80 nm in thickness, and stained them with uranyl acetate and lead citrate. We viewed grids on a Siemans 101 electron microscope at an accelerating voltage of 80 kV.

Co-immunoprecipitation and yeast two-hybrid analyses. We fused open reading frames of *ru*, *ru2*, *pe* and *STAT3* cDNA in frame to pCMV-Tag vectors (Myc and Flag), and verified the identities of the resulting fusion constructs by sequencing. We co-transfected 1.5×10^5 COS-7 cells, using FUGENE6 (Roche), with epitope-tagged constructs at a ratio of 1:1, except in the cases of ru-Flag and ru2-Flag with STAT3-Myc (1.9:0.1) and ru2-flag with ru-Myc (1.8:0.2). At 48 h after transfection, we solubilized proteins with 50 mM Tris-HCl, pH 7.4,150 mM NaCl,1 mM EDTA,1% Triton X-100 and protease inhibitors for 1 h at 4 °C. We immunoprecipitated samples by incubating them for 1 h at 4 °C with Flag M2 antibody–conjugated agarose (Sigma), and washed the agarose beads three times with 0.5 M Tris-HCl, pH 7.4, plus 1.5 M NaCl. We eluted bound proteins by treating the samples for 5 min at 95 °C with denaturing Laemmli buffer, and analyzed blots of 8% SDS-PAGE gels either with rabbit polyclonal antibody against Flag (1:1,000 dilution; Affinity Bio-Reagents) or with rabbit polyclonal antibody against Myc (1:200 dilution; Santa Cruz). We used horseradish peroxidase–linked donkey antibody against rabbit immunoglobulin G (1:4,000 dilution; Amersham Life Sciences) as a secondary antibody for all blots. The blots shown are representative of at least three independent experiments.

We used the Matchmaker GAL4 Two-Hybrid System 3 kit (Clontech) for two-hybrid analyses. We fused full-length *ru2*, *ru* or *coa* (*HPS3*) cDNA in-frame to the DNA binding (pGBKT7) and activation (pGADT7) domains of the *GAL4* transcription factor, and verified resulting fusion constructs by sequencing. We co-transformed fusion constructs into *Saccharomyces cerevisiae* strain AH109 and suspended at least two colonies of each double transformant growing on low-stringency medium (lacking Trp and Leu) in low-stringency broth for growth at 30 °C on a shaker for 16 h. We adjusted cell cultures to 0.4 optical density at 600 nm, and applied 3 µl from each co-transformation to low-stringency and high-stringency (lacking Trp, Leu, His and adenine) plates containing X-α-GAL. We incubated plates at 30 °C for 5 d and monitored the samples for growth and blue color.

GenBank accession numbers. Mouse *ru2* cDNA sequences: AF534396, AF534397, AF534398, AF534399. Human *HPS5* sequences: AF534400, AF534401, AF534402. Mouse *ru* sequence: AF536239. Human *HPS6* sequence: AF536238.

Note: Supplementary information is available on the Nature Genetics website.

Acknowledgments

We thank M. Reddington, L. Zhen, Y. Jiang, D. Poslinski, D. Tabaczynski, M. Ellsworth, J. Pazik, and J. Tan for technical assistance; D. Swing for the microinjection; L. Gagnon for helping with the JE/Le cross; Y. Ni, X. Jiang and L. Song for sequencing BACs; and H. Chen for assistance in 5′RACE analysis of ru2. P. Graf, C. McGregor and D. Ako-Adjei contributed to the construction of the ru genetic map. We thank H. Baumann for the gift of the STAT3 construct. This work was supported in part by the National Institutes of Health (R.T.S., E.M.E., B.A.R. and R.A.S.) and by the National Cancer Institute, Department of Health and Human Services (N.G.C. and N.A.J.). This research used core facilities supported in part by Roswell Park Cancer Institute's National Cancer Institute–funded Cancer Center Support Grant and by the Cancer Core Grant of The Jackson Laboratory.

Competing interests statement

The authors declare that they have no competing financial interest.

Received 5 September 2002; accepted 3 January 2003.

1. Huizing, M., Anikster, Y. & Gahl, W.A. Hermansky-Pudlak syndrome and Chediak-Higashi syndrome: Disorders of vesicle formation and trafficking. *Thromb. Haemost.* **86**, 233–245 (2001).
2. Spritz, R.A. Multi-organellar disorders of pigmentation: Tied up in traffic. *Clin. Genet.* **55**, 309–317 (1999).
3. Gardner, J.M. *et al*. The mouse pale ear *(ep)* mutation is the homologue of human Hermansky-Pudlak syndrome (HPS). *Proc. Natl. Acad. Sci. USA* **94**, 9238–9243 (1997).
4. Feng, G.H., Bailin, T., Oh, J. & Spritz, R.A. Mouse pale ear (*ep*) is homologous to human Hermansky-Pudlak syndrome and contains a rare 'AT-AC' intron. *Hum. Molec. Genet.* **6**, 793–797 (1997).
5. Oh, J. *et al*. Positional cloning of a gene for Hermansky-Pudlak syndrome, a disorder of cytoplasmic organelles. *Nat. Genet.* **14**, 300–306 (1996).
6. Feng, L. *et al*. The β3A subunit gene *(Ap3b1)* of the AP-3 adaptor complex is altered in the mouse hypopigmentation mutant pearl, a model for Hermansky-Pudlak Syndrome and night blindness. *Hum. Molec. Genet.* **8**, 323–330 (1999).
7. Dell'Angelica, E.C., Shotelersuk, V., Aguilar, R.C., Gahl, W.A. & Bonifacino, J.S. Altered trafficking of lysosomal proteins in Hermansky-Pudlak syndrome due to mutations in the β3A subunit of the AP-3 adaptor. *Mol. Cell* **3**, 11–21 (1999).
8. Suzuki, T. *et al*. The gene mutated in cocoa mice, carrying a defect of organelle biogenesis, is a homologue of the human Hermansky-Pudlak syndrome-3 gene. *Genomics* **78**, 30–37 (2001).
9. Anikster, Y. *et al*. Mutation of a new gene causes a unique form of Hermansky-Pudlak syndrome in a genetic isolate of central Puerto Rico. *Nat. Genet.* **28**, 376–380 (2001).
10. Suzuki, T. *et al*. Hermansky-Pudlak syndrome is caused by mutations in *HPS4*, the human homolog of the mouse light-ear gene. *Nat. Genet.* **30**, 321–324 (2002).
11. Swank, R.T., Novak, E.K., McGarry, M.P., Rusiniak, M.E. & Feng, L. Mouse models of Hermansky-Pudlak syndrome: A review. *Pig. Cell Res.* **11**, 60–80 (1998).
12. Swank, R.T., Novak, E.K., McGarry, M.P., Zhang, Q. & Feng, L. Abnormal vesicular trafficking in mouse models of Hermansky-Pudlak syndrome. *Pig. Cell Res.* **13**, 59–67 (2000).
13. Silvers, W.K. *The Coat Colors of Mice: A Model for Mammalian Gene Action and Interaction* 103–104 (Springer-Verlag, New York, 1979).
14. Dunn, L.C. A new eye color mutant in the mouse with asymmetrical expression. *Proc. Natl. Acad. Sci.* **31**, 343–346 (1945).
15. Eicher, E.M. The position of *ru2* and *qv* with respect to the flecked translocation in the mouse. *Genetics* **64**, 495–510 (1969).
16. Eicher, E.M. & Fox, S. *Mouse News Lett.* **56**, 42 (1977).
17. Novak, E.K., Wieland, F., Jahreis, G.P. & Swank, R.T. Altered secretion of kidney lysosomal enzymes in the mouse pigment mutants ruby-eye, ruby-eye-2-J and maroon. *Biochem. Genet.* **18**, 549–561 (1980).
18. Novak, E.K., Hui, S.-W. & Swank, R.T. Platelet storage pool deficiency in mouse pigment mutations associated with seven distinct genetic loci. *Blood* **63**, 536–544 (1984).
19. Oberhauser, A.F. & Fernandez, J.M. A fusion pore phenotype in mast cells of the ruby-eye mouse. *Proc. Natl. Acad. Sci.* **93**, 14349–14354 (1996).
20. Russell, L.B., Montgomery, C.S., Cacheiro, N.L. & Johnson, D.K. Complementation analyses for 45 mutations encompassing the pink-eyed dilution (*p*) locus of the mouse. *Genetics* **141**, 1547–1563 (1995).
21. O'Brien, E.P. *et al*. Molecular map of chromosome 19 including three genes affecting bleeding time: *ep, ru* and *bm*. *Mammal. Genome* **5**, 356–360 (1994).
22. Lee, S.T., Park, S.K., Lee, K.H., Holmes, S.M. & Spritz, R.A. A non-radioactive method or simultaneous detection of single-strand conformation polymorphisms (SSCPs) and heteroduplexes. *Mol. Cells* **5**, 668–672 (1995).
23. Zhang, Q. *et al*. The gene for the muted (*mu*) mouse, a model for Hermansky-Pudlak Syndrome, defines a novel protein which regulates vesicle trafficking. *Hum. Mol. Genet.* **11**, 697–706 (2002).
24. Kantheti, P. *et al*. Mutation in AP-3 delta in the *mocha* mouse links endosomal transport to storage deficiency in platelets, melanosomes and synaptic vesicles. *Neuron* **21**, 111–122 (1998).
25. Robinson, M.S. & Bonifacino, J.S. Adaptor-related proteins. *Curr. Opin. Cell. Biol.* **13**, 444–453 (2001).
26. Detter, J.C. *et al*. Rab geranylgeranyl transferase-α mutation in the gunmetal mouse reduces Rab prenylation and platelet synthesis. *Proc. Natl. Acad. Sci. USA* **97**, 4144–4149 (2000).
27. Wilson, S.M. *et al*. A mutation in *Rab27a* causes the vesicle transport defects observed in *ashen* mice. *Proc. Natl. Acad. Sci. USA* **97**, 7933–7938 (2000).
28. Wu, X., Wang, F., Rao, K., Sellers, J.R. & Hammer, J.A.R. Rab27a is an essential component of melanosome receptor for myosin Va. *Mol. Biol. Cell* **13**, 1735–1749 (2002).
29. Strom, M., Hume, A.N., A.K., T., Barkagianni, E. & Seabra, M.C. A family of Rab27-binding proteins. Melanophilin links Rab27a and myosin Va function in melanosome transport. *J. Biol. Chem.* **277**, 25423–25430 (2002).
30. Kuroda, T.S., Fukuda, M. & Mikoshiba, K. The Slp homology domain of synaptotagmin-like proteins 1–4 and Slac2 functions as a novel Rab27a binding domain. *J. Biol. Chem.* **277**, 9212–9218 (2002).
31. Novak, E.K. *et al*. The regulation of platelet-dense granules by Rab27a in the ashen mouse, a model of Hermansky-Pudlak and Griscelli syndromes, is granule-specific and dependent on genetic background. *Blood* **100**, 128–135 (2002).
32. Suzuki, T. *et al*. The mouse organellar biogenesis mutant buff (*bf*) results from a mutation in *Vps33a*, a homologue of yeast *vps33* and Drosophila carnation (*car*). *Proc. Natl. Acad. Sci. USA* (in the press).

33. Huang, L., Kuo, Y.-M. & Gitschier, J. The pallid gene encodes a novel, syntaxin 13-interacting protein involved in platelet storage pool deficiency. *Nat. Genet.* **23**, 329–332 (1999).
34. Falcon-Perez, J.M., Starcevic, M., Gautam, R. & Dell'Angelica, E.C. BLOC-1, a novel complex containing the pallidin and muted proteins involved in the biogenesis of melanosomes and platelet-dense granules. *J. Biol. Chem.* **277**, 28191–28199 (2002).
35. Moriyama, K. & Bonifacino, J.S. Pallidin is a component of a multi-protein complex involved in the biogenesis of lysosome-related organelles. *Traffic* **3**, 666–677 (2002).
36. Meisler, M.H., Wanner, L., & Strahler, J. Pigmentation and lysosomal phenotypes in mice doubly homozygous for both light-ear and pale-ear mutant alleles. *J. Hered.* **75**, 103–106 (1984).
37. Oh, J. *et al*. The Hermansky-Pudlak syndrome (HPS) protein is part of a high molecular weight complex involved in biogenesis of early melanosomes. *Hum. Mol. Genet*. **9**, 375–385 (2000).
38. Wixler, V. *et al*. Identification of novel interaction partners for the conserved membrane proximal region of α-integrin cytosplasmic domains. *FEBS Lett.* **445**, 351–355 (1999).
39. Moore, K.J., Swing, D.A., Copeland, N.G. & Jenkins, N.A. Interaction of the murine dilute suppressor gene (*dsu*) with fourteen coat color mutations. *Genetics* **125**, 421–430 (1990).
40. Feng, L. *et al*. The Hermansky-Pudlak syndrome 1 (HPS1) and HPS2 genes independently contribute to the production and function of platelet dense granules, melanosomes, and lysosomes. *Blood* **99**, 1651–1658 (2002).
41. Bodenteich, A., Chissoe, S., Wang, Y.F. & Roe, B.A. Shotgun cloning as the strategy of choice to generate templates for high throughput dideoxynucleotide sequencing. in *Automated DNA Sequencing and Analysis Techniques* eds. Adams, M.D., Fields, C. and Venter, C. 42–50 (Academic Press, London, 1994).
42. Chissoe, S.L. *et al*. Strategies for rapid and accurate DNA sequencing. in *Methods: A Companion to Methods in Enzymology*, Vol. 3 ed. Roe. B.A. (Academic Press, New York 1991).